

Shifting the Sweet Spot: High-Performance Matrix-Free Method for High-Order Elasticity

DALI CHANG, Dalian University of Technology, China

CHONG ZHANG, Institute of Software Chinese Academy of Sciences, China and University of the Chinese Academy of Sciences, China

KAIQI ZHANG, Dalian University of Technology, China

MINGGUAN YANG, National Technology Innovation Center of Guangdong-Hong Kong-Macao Greater Bay Area, China

HUIYUAN LI*, Institute of Software Chinese Academy of Sciences, China

WEIQIANG KONG†, Dalian University of Technology, China

In high-order finite element analysis for elasticity, matrix-free (PA) methods are a key technology for overcoming the memory bottleneck of traditional Full Assembly (FA). However, existing implementations fail to fully exploit the special structure of modern CPU architectures and tensor-product elements, causing their performance "sweet spot" to anomalously remain at the low order of $p \approx 2$, which severely limits the potential of high-order methods. To address this challenge, we design and implement a highly optimized PA operator within the MFEM framework, deeply integrated with a Geometric Multigrid (GMG) preconditioner. Our multi-level optimization strategy includes replacing the original $O(p^6)$ generic algorithm with an efficient $O(p^4)$ one based on tensor factorization, exploiting Voigt symmetry to reduce redundant computations for the elasticity problem, and employing macro-kernel fusion to enhance data locality and break the memory bandwidth bottleneck. Extensive experiments on mainstream x86 and ARM architectures demonstrate that our method successfully shifts the performance "sweet spot" to the higher-order region of $p \geq 6$. Compared to the MFEM baseline, the optimized core operator (kernel) achieves speedups of 7x to 83x, which translates to a 3.6x to 16.8x end-to-end performance improvement in the complete solution process. This paper provides a validated and efficient practical path for conducting large-scale, high-order elasticity simulations on mainstream CPU hardware.

CCS Concepts: • Mathematics of computing → Mathematical software performance; Solvers; • Applied computing → Computer-aided design; • Computing methodologies → Shared memory algorithms.

Additional Key Words and Phrases: Matrix-Free, Geometric Multigrid, Sum-Factorization, Elasticity, MFEM

1 Introduction

In high-precision scientific and engineering computing, high-order Finite Element Methods (FEM) are a powerful tool for solving Partial Differential Equations (PDEs), owing to their ability to achieve exponential convergence rates with fewer degrees of freedom [15, 22, 32]. In key applications such as linear elasticity, the finite element discretization ultimately leads to a large-scale sparse linear system, $\mathbf{A}\mathbf{x} = \mathbf{b}$. As the primary means of solving such systems, the

*Corresponding author

†Corresponding author

New Paper, Not an Extension of a Conference Paper.

Authors' Contact Information: Dali Chang, changdali@mail.dlut.edu.cn, Dalian University of Technology, Dalian, Liaoning, China; Chong Zhang, zhangchong2020@iscas.ac.cn, Institute of Software Chinese Academy of Sciences, Beijing, China and University of the Chinese Academy of Sciences, Beijing, China; Kaiqi Zhang, zhangkq@mail.dlut.edu.cn, Dalian University of Technology, Dalian, Liaoning, China; Mingguan Yang, yangmingguan@ncti-gba.cn, National Technology Innovation Center of Guangdong-Hong Kong-Macao Greater Bay Area, Guangzhou, Guangdong, China; Huiyuan Li, huiyuan@iscas.ac.cn, Institute of Software Chinese Academy of Sciences, Beijing, China; Weiqiang Kong, wqkong@dlut.edu.cn, Dalian University of Technology, Dalian, Liaoning, China.

execution efficiency of the core computation in iterative methods—the matrix-vector product (Mat-Vec)—dominates the overall runtime of the entire simulation, becoming the critical performance bottleneck.

There are two strategies for implementing the matrix-vector product: Full Assembly (FA) and Partial Assembly (PA). For high-order finite elements, the FA strategy suffers from a severe "memory wall" bottleneck due to its exponentially growing memory consumption, severely limiting its application. In response, the PA (or matrix-free) method computes the action of the matrix on a vector "on-the-fly" instead of storing the matrix, successfully transforming the problem from being memory-access-intensive to compute-intensive and opening a path to leverage the formidable arithmetic capabilities of modern multi-core processors[28]. Against this backdrop, PA methods based on tensor-product elements (quadrilaterals/hexahedra) have garnered significant attention for their dominant role in geometric modeling[21, 33, 34] and their unparalleled performance potential [9, 24, 30, 38]. Their tensor-product structure allows the use of the sum-factorization technique to reduce the complexity of the operator application on a 3D element from $O(p^6)$ to $O(p^4)$, making it the theoretically optimal path for unleashing the computational power of modern processors.

However, despite this significant theoretical advantage, existing implementations are far from translating this potential into practical performance, especially for complex physics problems on modern multi-core CPUs. First, much of the high-performance research on PA methods has focused on relatively simple scalar problems, such as the Poisson equation [25, 26, 29]. When transitioning to vector problems like elasticity, the need to handle more complex constitutive relations (e.g., the contraction of the elasticity tensor C_{ijkl}) presents unique performance challenges in managing arithmetic intensity and data locality[19, 27]. Second, although some studies have achieved significant performance gains in elastic computing by leveraging massively parallel accelerators such as GPUs[8, 17, 36], optimizing for modern mainstream CPU architectures remains a hot topic in many research areas[40]. This performance gap on CPUs is evident across the software ecosystem. On one hand, general-purpose frameworks like MFEM[2] and deal.ii[4], while providing matrix-free solvers for elasticity, often prioritize generality and modularity at the expense of extreme optimization for the tensor-product structure. On the other hand, even within the performance-oriented libCEED library [7], research by Mehrabian et al[31]. has explicitly shown that the performance "sweet spot" on CPU platforms anomalously appears at lower polynomial degrees, such as $p = 2$ or $p = 3$. These observations collectively point to a clear research gap: the lack of a systematic optimization strategy and integrated solution capable of genuinely pushing the performance sweet spot of the elasticity PA operator to high orders ($p \gg 3$) on modern high-performance CPUs.

Furthermore, an efficient operator alone does not constitute a high-performance solver; any meaningful operator optimization must be validated within its final solver context, such as those provided by comprehensive scientific computing frameworks like PETSc[5]. The matrix-free nature of the PA method makes it inherently incompatible with algebraic preconditioners (such as AMG or incomplete factorizations) that rely on explicit matrix entries, which are cornerstone features of highly-optimized preconditioning libraries like hypre[16]. Among the few compatible options, Geometric Multigrid (GMG) stands out for its near-optimal computational complexity and excellent parallel scalability[13]. More importantly, the core components of GMG—the smoother/relaxation operators (e.g. Jacobi or Chebyshev iteration)—can themselves be implemented in a matrix-free fashion. This forms an ideal synergy with the PA method and is recognized as one of the best practices for working in concert with PA methods [8, 26].The core objective of this paper is precisely to address the aforementioned disconnect between theory and practice by deeply optimizing the PA operator and integrating it end-to-end with a GMG preconditioner, thereby unleashing the full potential of high-order finite element methods in practice.

To this end, this paper is dedicated to building a highly optimized PA core operator for tensor-product elements within the MFEM framework and combining it with a Geometric Multigrid preconditioner to unleash the full potential of solving high-order elasticity problems. The main contributions of this work are as follows:

- (1) **A Multi-Level PA Operator Optimization Strategy for High-Order Elasticity:** We build our high-performance operator upon a modern, tensor-factorization-based $O(p^4)$ algorithm to complement the native $O(p^6)$ operator in MFEM, which was designed for generality. Furthermore, we systematically address performance bottlenecks in the elasticity PA operator by combining optimizations using Voigt symmetry with macro-kernel fusion techniques.
- (2) **An Integrated and Validated GMG-PA Solver:** To validate the effectiveness of our optimized PA operator, we build a complete matrix-free solution scheme within MFEM for linear elasticity that is deeply integrated with a GMG preconditioner, addressing the practical application of the PA operator within a high-performance solver.
- (3) **Systematic Demonstration of Performance Advantages:** Experiments prove that our method not only comprehensively outperforms traditional FA and the baseline PA in MFEM but, more importantly, successfully shifts the performance "sweet spot" on CPUs from the previously observed $p = 2$ to $p = 6$ and beyond, providing a validated and efficient practical solution for large-scale, high-order elasticity problems.

The remainder of this paper is organized as follows. Section 2 reviews the governing equations for linear elasticity, its finite element discretization, and compares the general-purpose and tensor-product-based PA implementation strategies. Section 3 details the architecture of our designed integrated GMG-MF solver. Section 4, the core of our optimization work, analyzes the performance bottlenecks of the matrix-free kernel and elaborates on the series of optimization techniques we employed. Section 5 presents exhaustive numerical experiments and performance comparison analyses. Finally, Section 6 concludes the paper and discusses future research directions.

2 Background: Mathematical Model and Numerical Discretization

This chapter establishes the mathematical and computational foundation for the high-performance operator optimizations presented in this paper. We begin by defining the finite element discretization for the linear elasticity problem. We then detail the two core implementation strategies introduced in the introduction—Full Assembly (FA) and Partial Assembly (PA)—and finally, describe sum-factorization on tensor-product elements, the key enabling technology for efficient PA. This material provides the necessary context for the performance bottleneck analysis and optimization strategies detailed in Section 4.

2.1 Governing Equations and Finite Element Discretization

The physical behavior of a deformable body under external forces, assuming small displacements, is governed by the equations of linear elasticity. The strong form of the static equilibrium problem, defined on a domain Ω , is given by the partial differential equation:

$$-\nabla \cdot \sigma(\mathbf{u}) = \mathbf{f} \quad \text{in } \Omega \quad (1)$$

where \mathbf{u} is the displacement field, \mathbf{f} is the body force vector, and σ is the Cauchy stress tensor. This system is completed by imposing Dirichlet and Neumann boundary conditions on the boundary $\Gamma = \partial\Omega$. The stress is related to the strain $\boldsymbol{\epsilon}(\mathbf{u}) = \frac{1}{2}(\nabla\mathbf{u} + (\nabla\mathbf{u})^T)$ through a constitutive model. For a general anisotropic material, this is a linear relationship

defined by a fourth-order elasticity tensor C . In component form, this relationship is expressed as:

$$\sigma_{ij} = \sum_{k=1}^3 \sum_{l=1}^3 C_{ijkl} \epsilon_{kl} \quad (2)$$

However, for the widely applicable case of isotropic materials, this relationship simplifies to Hooke's Law:

$$\sigma(\mathbf{u}) = \lambda(\nabla \cdot \mathbf{u})\mathbf{I} + 2\mu\epsilon(\mathbf{u}) \quad (3)$$

where λ and μ are the Lamé material parameters and \mathbf{I} is the identity tensor[6].

The Finite Element Method (FEM) is the standard approach for solving this problem. It begins by recasting the strong form Eq. (1) into an equivalent integral weak form: find $\mathbf{u} \in V$ such that for all test functions $\mathbf{v} \in V$:

$$\underbrace{\int_{\Omega} \sigma(\mathbf{u}) : \epsilon(\mathbf{v}) d\Omega}_{a(\mathbf{u}, \mathbf{v})} = \underbrace{\int_{\Omega} \mathbf{f} \cdot \mathbf{v} d\Omega + \int_{\Gamma_N} \mathbf{g} \cdot \mathbf{v} d\Gamma}_{L(\mathbf{v})} \quad (4)$$

Here, V is a suitable Sobolev space, $a(\mathbf{u}, \mathbf{v})$ is a symmetric bilinear form representing the internal virtual work, and $L(\mathbf{v})$ is a linear form for the external virtual work. It is noteworthy that since the stress tensor $\sigma(\mathbf{u})$ is symmetric, its double dot product with any tensor (here, $\nabla \mathbf{v}$) is equivalent to its product with that tensor's symmetric part ($\epsilon(\mathbf{v})$), leading to the alternative form $a(\mathbf{u}, \mathbf{v}) = \int_{\Omega} \sigma(\mathbf{u}) : \nabla \mathbf{v} d\Omega$. This form highlights the direct relationship between the stress tensor and the gradient of the test function.

To make the problem computationally tractable, the continuous domain Ω is discretized into a mesh of elements, and the infinite-dimensional space V is approximated by a finite-dimensional subspace V_h . The solution \mathbf{u} is then approximated as $\mathbf{u}_h = \sum_{j=1}^N \mathbf{U}_j \phi_j$, where $\{\phi_j\}$ are the finite element basis functions (shape functions) and \mathbf{U} is the global vector of unknown nodal displacements. Applying the Galerkin principle, this discretization transforms the weak form Eq. (4) into a large, sparse system of linear equations:

$$\mathbf{A}\mathbf{U} = \mathbf{F} \quad (5)$$

where \mathbf{A} is the global stiffness matrix, \mathbf{U} is the global vector of degrees of freedom, and \mathbf{F} is the global load vector. The entries of the stiffness matrix are assembled from elemental contributions, where each entry A_{ij} is computed from the bilinear form $a(\phi_i, \phi_j)$ [15, 22, 32]. For efficient computational implementation, the tensor operations within this integral are typically mapped to matrix-vector operations using Voigt notation, which re-represents the symmetric stress and strain tensors as 6-dimensional vectors. For instance, the strain vector is given by $\boldsymbol{\epsilon}_{\text{voigt}} = [\epsilon_{11}, \epsilon_{22}, \epsilon_{33}, 2\epsilon_{23}, 2\epsilon_{13}, 2\epsilon_{12}]^T$. With this notation, the constitutive model Eq. (2) can be expressed as a matrix-vector product $\boldsymbol{\sigma}_{\text{voigt}} = \mathbf{C}\boldsymbol{\epsilon}_{\text{voigt}}$, where \mathbf{C} is a 6×6 material stiffness matrix. This matrix representation is fundamental to the construction of the global stiffness matrix \mathbf{A} .

The resulting global stiffness matrix \mathbf{A} in Eq. (5) is sparse, symmetric, and positive-definite (SPD). For large-scale problems, such systems are almost exclusively solved using iterative methods, with the Conjugate Gradient (CG) algorithm being the method of choice. The performance of the CG solver is dominated by the computation of the sparse matrix-vector product (SpMV) in each iteration. Therefore, the efficiency of this kernel operation is paramount and directly dictates the time-to-solution for the entire simulation.

2.2 High-Performance Computing Strategies for FEM Operators

When solving the linear system $AU = F$ with an iterative method, the computational bottleneck is the repeated matrix-vector product. To fully understand its optimization potential, we must examine the components of the global discrete operator A . From a mathematical perspective, the global operator A can be viewed as a chain of discrete operators, as expressed in libraries like MFEM: $A = P^T G^T B^T D B G P$ [2, 3]. As shown in Figure 1, each operator in this chain has a distinct physical and mathematical meaning: P , the subdomain restriction operator, which maps global degrees of freedom to local degrees of freedom for each subdomain; G , the element restriction operator, which maps local subdomain degrees of freedom to the degrees of freedom for each element within that subdomain; B , the basis function evaluation operator, which transforms the degrees of freedom on each element to function values at the quadrature points within that element; and D , the quadrature point operator, which applies the physical operator and integration weights at the quadrature points. The core of designing a high-performance solver lies in choosing the most efficient strategy to execute this operator chain, which has given rise to two fundamentally different technological paths: Full Assembly and Matrix-Free methods.

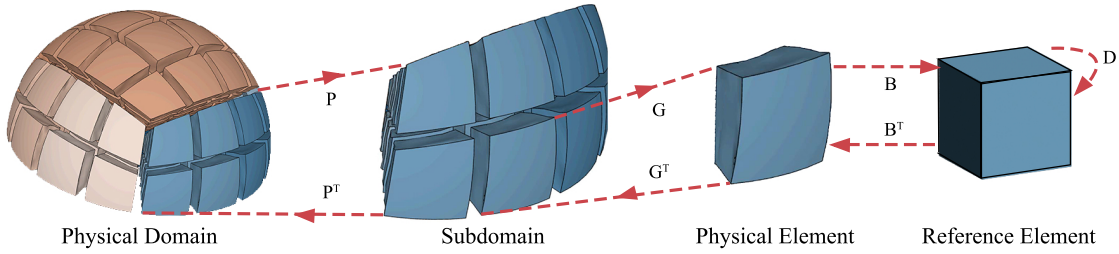


Fig. 1. Conceptual decomposition of the FEM operator into a chain of discrete operators, as implemented in libraries like MFEM.

2.2.1 Full Assembly. Full Assembly is the traditional implementation method in finite element analysis. It opts to pre-compute and store the final result of the entire operator chain—the global stiffness matrix A —before the solution process begins. This is accomplished by iterating through all mesh elements, explicitly calculating each local matrix, and then assembling them into a single, large global sparse matrix. In the subsequent iterative solve, each matrix-vector multiplication is simplified to a standard Sparse Matrix-Vector multiplication (SpMV) operation. However, for high-order finite elements, this "compute-first, use-later" strategy leads to a severe "memory wall" bottleneck on modern computational architectures. This bottleneck manifests in two critical ways. First, it presents a capacity wall: as the element polynomial degree p increases, the number of non-zero entries in the global matrix A grows explosively. The resulting memory footprint often exceeds the capacity of a single compute node, fundamentally limiting the scale of the problem that can be solved. Furthermore, even if the matrix fits in memory, performance is constrained by a bandwidth wall. The SpMV operation is a classic memory-bound computation. Its arithmetic intensity—the number of floating-point operations performed per byte of data accessed from memory—is typically far too low to "feed" the powerful computational units of modern CPUs and GPUs [12, 20]. Its inherently indirect and irregular memory access patterns also severely hinder cache efficiency, leading to a significant waste of the hardware's peak computational performance.

2.2.2 Matrix-Free (PA). Matrix-free methods, or Partial Assembly (PA), adopt the opposite philosophy. They recognize that an iterative solver only requires the *action* of the operator A on a vector \mathbf{u} , not the matrix A itself. The PA strategy,

therefore, opts to dynamically compute the operator chain. That is, each time the product $\mathbf{y} = \mathbf{A}\mathbf{u}$ is needed, the full sequence of operations $\mathbf{y} = (P^T G^T B^T D B G P)\mathbf{u}$ is executed "on-the-fly," without ever explicitly forming or storing the global matrix \mathbf{A} [10, 11, 29]. This "just-in-time" computation strategy trades increased arithmetic workload for a minimal memory footprint, making it possible to solve large-scale, high-order problems. However, this introduces a new core challenge: without optimization, the immense computational cost of evaluating the operator chain becomes a new performance bottleneck. A naive matrix-free implementation for 3D high-order elements can have a computational complexity of $O(p^6)$, which is infeasible in practice [24]. Consequently, efficient matrix-free methods must rely on specialized algorithms to reduce this computational complexity.

2.2.3 Tensor-Product Sum-Factorization. Fortunately, for the quadrilateral and hexahedral elements that dominate engineering and scientific computing, the high-order basis functions possess a special tensor-product structure, which is the key to enabling efficient matrix-free methods. A 3D basis function $\Phi(\xi, \eta, \zeta)$ can be expressed as the product of three 1D basis functions $\phi(r)$:

$$\Phi_{ijk}(\xi, \eta, \zeta) = \phi_i(\xi) \cdot \phi_j(\eta) \cdot \phi_k(\zeta) \quad (6)$$

This structure allows us to decompose high-dimensional operators into a series of operations on 1D components. Sum-factorization is the technique that leverages this principle to reformulate a single, high-dimensional, and expensive tensor contraction into an equivalent series of low-dimensional, inexpensive matrix operations. Conceptually, the action of a 3D gradient operator, G_{3D} , can be decomposed into the sum of contributions from the three spatial directions. For example, the partial derivative operator in the ξ direction, G_ξ , can be represented as a Kronecker product of 1D operator matrices: $G_\xi = \mathbf{D}_{1D} \otimes \mathbf{B}_{1D} \otimes \mathbf{B}_{1D}$, where \mathbf{D}_{1D} is the 1D derivative operator and \mathbf{B}_{1D} is the 1D interpolation operator. The essence of sum-factorization is that instead of explicitly forming and storing the large dense matrices defined by the Kronecker products, their action is implemented equivalently through a sequence of 1D matrix multiplications [1, 15, 32]. It is this "factorized evaluation" strategy that reduces the complexity of applying a local operator from $O(p^{2d})$ to $O(d \cdot p^{d+1})$, which in the 3D case means a drastic reduction in computational complexity from $O(p^6)$ to $O(p^4)$. This algorithmic optimization profoundly changes the nature of the computation: it transforms what could be a memory-bandwidth-limited operation into a series of compute-intensive kernels with high data locality. This computational pattern perfectly aligns with the cache hierarchies and SIMD/SIMT parallelism of modern CPUs and GPUs. Therefore, high-order FEM combining matrix-free methods with sum-factorization techniques represents a key technological path for achieving large-scale, high-fidelity scientific computing on modern HPC platforms.

3 Architecture of the Geometric Multigrid Preconditioner

As established in the introduction, a high-performance iterative solver requires optimizing both the time per iteration (via an efficient operator) and the total number of iterations (via a powerful preconditioner). This chapter details the architecture of our solver, which integrates a Geometric Multigrid (GMG) preconditioner with the Partial Assembly (PA) method to achieve this balance. Although demonstrated for the linear elasticity problem, the design principles are general and can be extended to other problems amenable to matrix-free methods. A standard GMG V-cycle consists of three core components: a smoother, inter-grid transfer operators, and a coarse-grid solver. The inter-grid transfer operators (restriction and prolongation) directly leverage the standard finite element interpolation operators provided by the MFEM library, which efficiently transfer data between different mesh levels. Given the specific requirements that matrix-free methods impose, the critical design decisions lie in the choice of the smoother and the coarse-grid solver. To ensure good convergence and scalability, our GMG framework employs a matrix-free smoother on the computationally

intensive fine grid levels, while switching to a more robust matrix-based solution strategy on the small-scale coarsest level.

3.1 Matrix-Free Smoothing with Chebyshev Polynomials

A key component of the multigrid cycle is the smoother, whose responsibility is to damp high-frequency components of the error. Traditional smoothers, such as Gauss-Seidel or SOR, require explicit access to the elements of the system matrix, which is impossible in our partial assembly framework. To overcome this well-known design challenge in matrix-free methods, we employ a Chebyshev polynomial smoother, which does not require global matrix information. This method constructs an effective smoothing process by applying a polynomial of the operator A to the residual, and its core advantage is that it only requires two inputs: the *action* of the matrix operator A and an estimate of the operator's spectral radius. The required maximum eigenvalue can be estimated efficiently at runtime using a few Lanczos or power iterations. The Chebyshev smoother is exceptionally well-suited for efficient implementation on modern parallel processors (e.g., GPUs), as its computations are dominated by vector updates and matrix-free operator applications—both of which map well to high-performance computational kernels. As described in recent work on MFEM, this approach aligns perfectly with our matrix-free philosophy, enabling effective error damping on fine grid levels while preserving the performance benefits of partial assembly.

3.2 Robust Coarse-Grid Solver

When the computation transitions to the coarsest level of the multigrid hierarchy, the problem characteristics change. At this point, the number of degrees of freedom is small enough that the overhead of explicit matrix assembly becomes negligible, while simultaneously, achieving a robust and accurate solution to the coarse-grid problem becomes critical for the convergence of the overall multigrid cycle. Therefore, on the coarsest grid, we adopt a hybrid strategy that transitions from matrix-free to matrix-based. We explicitly assemble the sparse stiffness matrix at this level and solve the resulting system using a powerful Algebraic Multigrid (AMG) preconditioner. The benefits of this hybrid approach are significant: it leverages the high throughput and low memory footprint of the matrix-free method on the computationally demanding fine grids, while capitalizing on the proven robustness and efficiency of AMG on the small-scale, yet convergence-critical, coarse grid. This ensures our GMG preconditioner is both fast and reliable.

By combining the components described above, we construct a complete, end-to-end preconditioner that employs different strategies for different algorithmic stages, as illustrated in Figure 2. It must be emphasized, however, that the ultimate performance ceiling of this solver is determined by the efficiency of its most computationally intensive part: the matrix-free PA operator. The next chapter, which constitutes the core of this paper, is therefore dedicated to a detailed, multi-level analysis of the performance optimization of this core operator.

4 High-Performance Sum-Factorization Operators for Geometric Multigrid

We now turn to the other angle of iterative solver optimization: reducing the time per iteration. This chapter details the series of optimization strategies we applied to the baseline Partial Assembly (PA) operator. Taking the kernel implementation in MFEM v4.8 as our starting point, we propose and implement a multi-level, synergistic optimization scheme. The cornerstone of this work is the replacement of the native, high-complexity operator with an efficient algorithm based on sum-factorization (Section 4.4), which provides the algorithmic foundation for order-of-magnitude performance gains. Subsequently, we introduce two critical performance-enhancing techniques: 1) exploiting Voigt notation to eliminate redundant computation and storage in the linear elasticity tensor (Section 4.3), and 2) reducing data

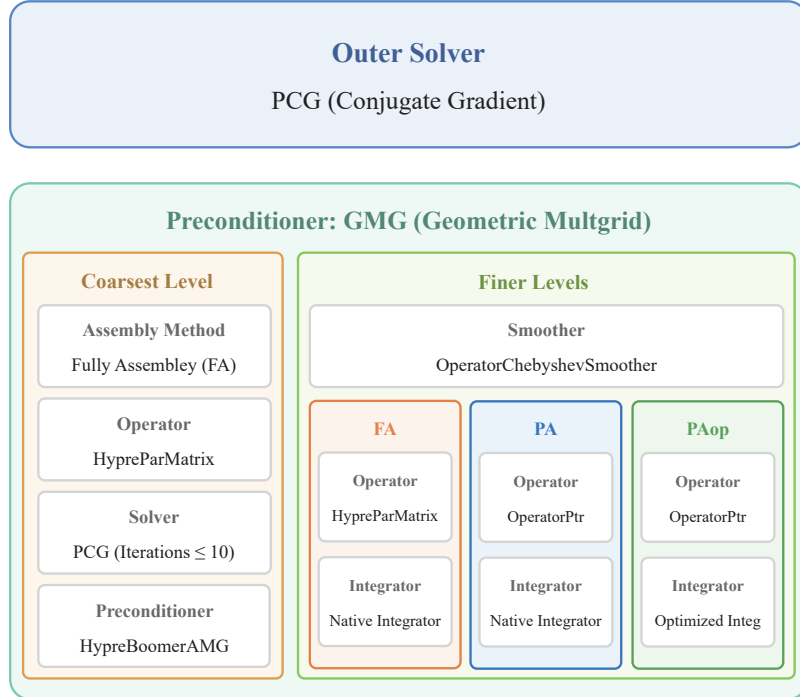


Fig. 2. Architecture of the hybrid Geometric Multigrid (GMG) preconditioner. On the fine grid levels (right), a matrix-free Chebyshev polynomial smoother is used. On the coarsest level (left), the system is explicitly assembled and solved robustly with an Algebraic Multigrid (AMG) preconditioner. FA, PA, and PAop all operate within this framework, differing only in operator type and whether the integrator is optimized.

movement and function call overhead through macro-kernel fusion (Section 4.2). Finally, to maximize data locality and overcome cache bottlenecks, we restructure the loop organization, designing a slice-wise fused computation strategy that transitions from "Fibers" to "Slices" (Section 4.5).

In the Finite Element Method, high-order elements (i.e., large polynomial degree p) can achieve equivalent accuracy with fewer Degrees of Freedom (DoFs), but at the cost of significantly increased computational complexity and memory requirements per element. In practice, the choice of p is a trade-off between application demands and computational cost: industry often uses lower orders ($p = 1$ or $p = 2$ [18]) to control costs, whereas cutting-edge academic research explores higher orders (e.g., $7 \leq p \leq 11$ [23]) in pursuit of ultimate efficiency. Considering memory footprint, arithmetic intensity, and the shifting trend of the performance "sweet spot," we select the range of $p = 1 - 8$ as the core optimization target for this study to systematically evaluate the performance of our strategies across different polynomial degrees.

4.1 Baseline Performance and Bottleneck Analysis

Any targeted optimization begins with a precise diagnosis of performance bottlenecks. To this end, we conducted an in-depth performance analysis of the standard matrix-free elasticity operator in MFEM v4.8. Results from tools like Intel VTune Profiler and Linux perf[14] were unequivocal: in a typical solve, the core matrix-vector multiplication function, `ElasticityAddMultPA`, consumed over 90% of the execution time, identifying it as the undisputed performance hotspot.

The logic of this baseline operator, shown in Algorithm 1, splits its core task of performing $\mathbf{y}+ = A(\mathbf{x})$ into two separate computational kernels. The first kernel iterates over all quadrature points to compute the stress tensor, writing the results to an intermediate array, QVec . The second kernel then iterates over all elements again, reading back the entire QVec array to perform a tensor contraction and accumulate the result. This two-stage, decoupled implementation reveals two fundamental performance flaws. First, it imposes a mandatory memory round-trip where the results of Kernel 1 are entirely "evicted" to main memory (DRAM), only to be read back in their entirety by Kernel 2, a process that completely destroys temporal data locality and creates a massive, unnecessary memory traffic bottleneck. Second, the operator application in Kernel 2 suffers from an extremely high computational cost, relying on a high-dimensional tensor contraction, $Y_{iqe+} = \sum_{p,m} \text{QVec}_{pmqe} \cdot G_{pmi}$, which has a prohibitively expensive computational complexity of $O(p^{2d})$ and requires streaming a massive basis gradient matrix G from main memory.

Algorithm 1 Baseline Operator

```

1: Input: Input vector  $X$ , Lamé parameters  $\lambda, \mu$ , geometry info  $\text{geom}$    Output: Output vector  $Y$ 
2:  $\text{QVec}_{\nabla u} \leftarrow \text{PhysDerivatives}((X))$                                  $\triangleright$  Compute physical gradients
3: // Kernel 1: Compute geometrically-transformed stress at quadrature points
4: for all each element  $e$  do
5:   for all each quadrature point  $p$  do                                          $\triangleright$  Load data for the current point
6:      $\nabla u \leftarrow \text{QVec}_{\nabla u}(p, e); \quad J \leftarrow \text{geom.J}(p, e); \quad w_p \leftarrow \text{ipWeights}[p]$ 
7:      $\boldsymbol{\epsilon}(u) \leftarrow \frac{1}{2}(\nabla u + (\nabla u)^T); \quad \boldsymbol{\sigma}(u) \leftarrow \lambda(p, e)(\nabla \cdot u)I + 2\mu(p, e)\boldsymbol{\epsilon}(u)$ 
8:      $\text{QVec}_{\sigma}(p, e) \leftarrow w_p \det(J) \cdot (J^{-T} \cdot \boldsymbol{\sigma}(u))$ 
9:   end for
10: end for
11: // Kernel 2: Apply operator action (gradient of test function)
12: for all each element  $e$  do
13:   for all  $i = 0$  to  $nDofs - 1$  and  $q = 0$  to  $d - 1$  do                                 $\triangleright$  Loop over test function DOFs
14:      $s \leftarrow \sum_{p=0}^{\text{numPoints}-1} \sum_{m=0}^{d-1} \text{QVec}_{\sigma}(p, m, q, e) \cdot G(p, m, i)$ 
15:      $Y(i, q, e) \leftarrow Y(i, q, e) + s$ 
16:   end for
17: end for

```

To quantify this bottleneck, we established a theoretical performance model. For a 3D problem ($d = 3$) using double precision, the asymptotic operational intensity of this operator approaches an extremely low constant of approximately 0.75 Ops/Byte. This extremely low operational intensity means, under the Roofline model, that the operator is architecturally destined to be memory-bandwidth-limited. Empirical data from Intel VTune Profiler and likwid[37] confirmed this, showing a measured operational intensity of approximately 0.87 Ops/Byte at $p = 8$, accompanied by a very high cache miss rate. This combined analysis indicates that our optimization must follow a two-pronged approach: first, break the kernel boundary to eliminate the macroscopic memory round-trip; then, within the fused kernel, reduce the complexity of the operator application at the algorithmic level.

4.2 Macro-kernel Fusion

To fundamentally solve the memory round-trip bottleneck, we designed and implemented a macro-kernel fusion strategy. The core idea is to restructure the program's overall dataflow, consolidating the multiple independent kernels—previously chained together via main memory—into a single, element-centric fused kernel. The baseline implementation consists of three conceptually separate, serial stages that exchange data through reads and writes to the global intermediate

array QVec: Gradient Interpolation, Stress Calculation, and Operator Action. Our fused kernel reconstructs this dataflow using an element-centric computation pattern, as shown in Algorithm 2. The entire operator application is placed within a single parallel loop that iterates over all finite elements.

Algorithm 2 Kernel Fusion

```

1: Input: Input vector  $X$ , Lamé parameters  $\lambda, \mu$ , geometry info geom   Output: Output vector  $Y$ 
2: for all each element  $e$  do
3:   for all  $p = 0$  to numPoints – 1 do
4:      $\nabla u_p \leftarrow \text{InterpolateGradAtPoint}(X, e, p)$ 
5:      $\sigma_p \leftarrow \text{CalculateStress}(\nabla u_p, \lambda_p, \mu_p)$ 
6:      $Q_p \leftarrow \text{TransformAndWeight}(\sigma_p, \text{geom}, p)$ 
7:   end for
8:   for all  $i = 0$  to nDofs – 1 do
9:      $Y_i \leftarrow \sum_{p=0}^{\text{numPoints}-1} \text{Contract}(Q_p, \text{GetBasisGradient}(i, p))$ 
10:     $Y(i, e) \leftarrow Y_i$ 
11:  end for
12: end for

```

For each element, all computational stages are executed sequentially, with intermediate data being staged in an on-chip buffer, el_QVec , sized for only a single element (e.g., ~51 KB for $d = 3, p = 8$) and small enough to reside entirely within the L1 or L2 cache. This approach yields significant performance advantages. Most importantly, it dramatically reduces global memory traffic, as reads and writes to the global QVec are eliminated and main memory access is strictly limited to the initial load of x and the final store of y . This fusion also enhances data locality by ensuring intermediate results are produced and consumed immediately within the high-speed cache, achieving excellent producer-consumer locality. Furthermore, merging multiple parallel regions into one avoids redundant synchronization points.

4.3 Optimizing Computation and Storage with Voigt Notation

After resolving the macroscopic data bottleneck with kernel fusion, our optimization focus shifted to the computational efficiency within the fused kernel. The baseline implementation operates on full $d \times d$ stress and strain tensors, but in linear elasticity, both are symmetric, leading to wasted storage and redundant floating-point operations. To eradicate this inefficiency, we leverage Voigt notation, which provides a lossless mapping from a symmetric 3×3 tensor to a 6-component vector. For our fused kernel, the direct benefit of this mapping is that the complex stress-strain relationship $\sigma = \mathbb{C} : \epsilon$ is transformed into an efficient 6×6 matrix-vector multiplication, as shown in the Eq. (6).

$$\begin{pmatrix} \sigma_{11} \\ \sigma_{22} \\ \sigma_{33} \\ \sigma_{23} \\ \sigma_{13} \\ \sigma_{12} \end{pmatrix} = \begin{pmatrix} \lambda + 2\mu & \lambda & \lambda & 0 & 0 & 0 \\ \lambda & \lambda + 2\mu & \lambda & 0 & 0 & 0 \\ \lambda & \lambda & \lambda + 2\mu & 0 & 0 & 0 \\ 0 & 0 & 0 & \mu & 0 & 0 \\ 0 & 0 & 0 & 0 & \mu & 0 \\ 0 & 0 & 0 & 0 & 0 & \mu \end{pmatrix} \begin{pmatrix} \epsilon_{11} \\ \epsilon_{22} \\ \epsilon_{33} \\ 2\epsilon_{23} \\ 2\epsilon_{13} \\ 2\epsilon_{12} \end{pmatrix} \quad (6)$$

This optimization delivers significant benefits on three levels. On a computational level, it simplifies the core constitutive model, reducing its floating-point operations by over 50%. On a memory level, it reduces the on-chip footprint of the el_QVec buffer by 33.3% by storing only the 6-component Voigt stress vector instead of the full 9-component tensor. Finally, on a dataflow level, applying Voigt notation throughout the entire chain streamlines the

data path, completely avoiding the generation of intermediate full 3×3 matrices and thereby reducing register pressure and unnecessary data movement.

4.4 Efficient Kernel Implementation for Sum-Factorization Operators

Kernel fusion and Voigt notation optimized the dataflow and redundant computations, but the $O(p^{2d})$ complexity of the operator application itself remained the ultimate bottleneck. To break through this barrier, we employ the sum-factorization technique, the theoretical principles of which were detailed in Section 2.2.3. We design and implement an efficient computational kernel that applies this theory to the tensor contraction process inherent in the operator. Specifically, our kernel reformulates a single, high-dimensional tensor contraction into an equivalent series of low-dimensional, small-scale tensor contractions (often matrix-matrix or matrix-vector multiplications), applying the operator on-the-fly. This algorithmic reconstruction, as realized in our implementation, achieves a fundamental reduction in complexity. In terms of memory access, this approach completely eliminates the need to read the massive G matrix, replacing it with access to small 1D basis and gradient matrices (B_{1D}, G_{1D}) that easily reside in the L1 cache. This removes the dominant term in memory access and reduces data transfer volume by orders of magnitude. In terms of computational cost, the complexity is significantly reduced from $O(d^2(p+1)^{2d})$ to $O(d^2 \cdot (p+1)^{d+1})$. For 3D problems, this represents a drop from $O((p+1)^6)$ to $O((p+1)^4)$ —a qualitative leap that serves as the algorithmic cornerstone for order-of-magnitude performance improvements.

4.5 Loop Structure Optimization for Data Locality: From Fibers to Slices

While sum-factorization is theoretically optimal, a naive implementation can expose new performance bottlenecks. Such an implementation naturally follows a fiber-wise data access pattern, as illustrated in Fig. 3(a), which conflicts severely with the cache hierarchy of modern CPUs. A phased, naive implementation would decompose the task into three separate loops (e.g., for contractions in X, Y, and Z), where each phase reads a large 3D intermediate tensor produced by the previous phase and writes another. This pattern introduces large, long-lived intermediate data structures that can be hundreds of kilobytes to several megabytes in size. If they spill from cache, the CPU is forced to shuttle data back and forth between slow main memory and fast execution units, causing severe cache thrashing and creating a memory-bound bottleneck that drastically limits performance.

To break this bottleneck, we completely reorganized the loop structure of the sum-factorization around a slice-wise computation strategy, as depicted in Fig. 3(b). The core idea is to shift the fundamental unit of computation from the entire 3D domain to a 2D slice of the output tensor. This new dataflow yields several crucial benefits. It completely eliminates the large 3D temporary arrays in favor of short-lived 2D arrays, enabling cache-resident computation where the entire producer-consumer chain for a given output slice is completed within the CPU’s high-speed cache. This, in turn, maximizes temporal locality, as intermediate data is reused before it can be evicted. The result is a computational pattern that keeps the arithmetic units continuously supplied with data, avoiding stalls and successfully shifting the performance bottleneck from memory access to floating-point computation itself.

Furthermore, this slice-wise strategy creates an ideal foundation for crucial low-level optimizations. First, by processing data slice-by-slice, the innermost loops naturally operate on contiguous memory blocks. We exploit this by ensuring proper memory alignment, which is a prerequisite for efficient SIMD vectorization and maximizing cache line utilization. Second, the computational independence of each slice makes the outer loop that iterates over them an ideal candidate for thread-level parallelism. This structural advantage opens up a clear path for future work on hybrid MPI+OpenMP parallelization, allowing for efficient execution on modern multi-core node architectures. Finally,

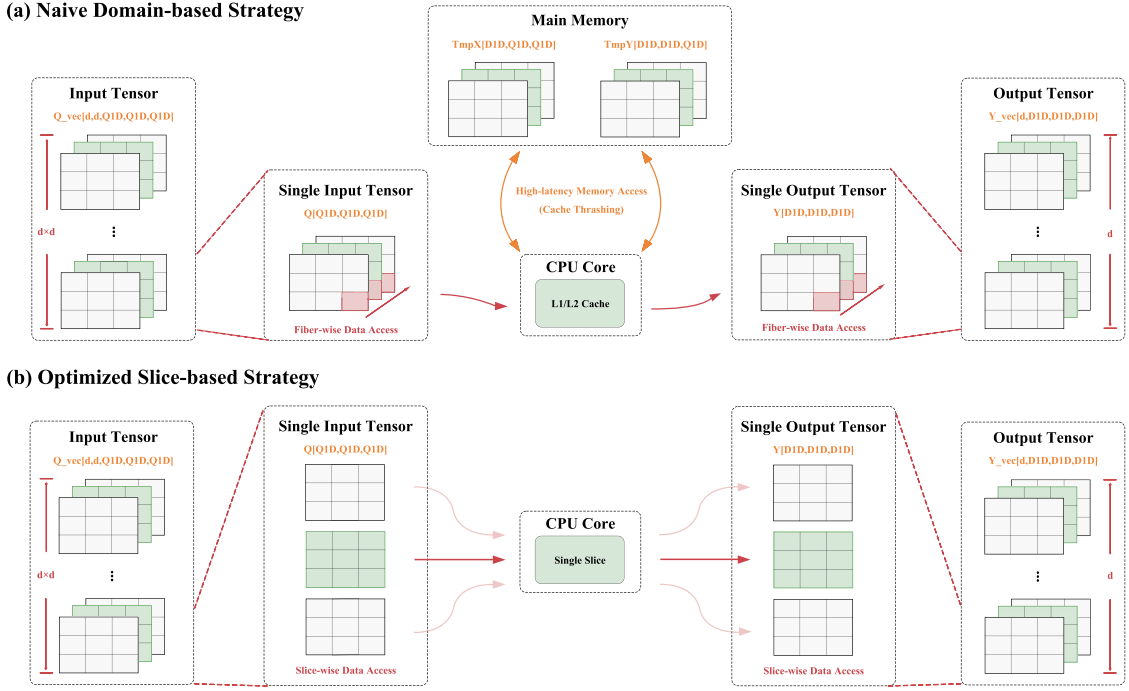


Fig. 3. Dataflow patterns for sum-factorization: (a) Naive fiber-wise pattern with large 3D intermediate tensors causing memory bottlenecks. (b) Optimized slice-wise pattern where computation is localized to cache-resident 2D slices, maximizing data locality.

within the computation of a single slice, the simplified loop structure allows for effective compiler-driven optimizations like loop unrolling and instruction scheduling, thereby maximizing instruction-level parallelism (ILP) and more fully exploiting the computational potential of a single core.

5 Experiments

To systematically evaluate the performance of FA, PA, and our proposed PAop method, we conducted a series of tests on both x86 and ARM hardware platforms. This section provides an in-depth analysis covering overall performance, memory consumption, and hardware efficiency.

5.1 Experimental Setup

This section details the hardware platforms, software environments, benchmark problem, and performance metrics used for our evaluation.

5.1.1 Hardware and Software Environment. We conducted performance evaluations on two representative yet architecturally distinct high-performance computing platforms to comprehensively assess the portability and effectiveness of our optimization methods. Platform A features a mainstream AMD EPYC (x86-64) architecture, while Platform B utilizes an ARM-based Huawei Kunpeng (AArch64) processor. All experiments were run with 64 MPI processes. Detailed hardware specifications and software configurations are provided in Table 1. We used MFEM (v4.8) as the foundational

library for our finite element computations. The theoretical memory bandwidth of the platforms was measured using the STREAM Triad benchmark from the likwid [37] tool, and peak computational performance (GFlop/s) was measured with the cpufp [35] tool to provide a realistic upper bound for hardware performance.

Table 1. Hardware and software specifications for the AMD and HiSilicon platforms.

	AMD EPYC 7713	HUAWEI Kunpeng 920 V200 7270Z
cores	2×64	1×64
base frequency	2.0GHz	2.9GHz
max frequency	3.675GHz	2.9GHz
L3 cache	4MB/core	1.75MB/core
SIMD width	256bit (AVX2)	128bit (NEON)+SVE
arithmetic peak	3027.44GFlop/s	2597.9GFlop/s
memory interface	DDR4-3200, 8 chan.	DDR5-4800, 8 chan.
Memory Size	256GB	512GB
STREAM memory bandwidth	124GB/s	180GB/s
Linux operating system release	Ubuntu 20.04	KylinSec OS Linux 3
compiler	gcc, version 13.3.1	gcc for openEuler 3.0.3
flags(-O3 -fopenmp)	-march=znver3 -mavx2 -mfma	-march=native -ffast-math

5.1.2 Methods Under Test. Within the Geometric Multigrid (GMG) preconditioning framework proposed in Section 3, we compare the performance of three distinct operator implementations. The first is **FA (Full Assembly)**, the traditional FEM implementation corresponding to `AssemblyLevel::FULL` in MFEM. The second is **PA (Partial Assembly)**, the standard matrix-free method corresponding to `AssemblyLevel::PARTIAL`. The third is **PAop (Optimized Partial Assembly)**, our proposed optimized matrix-free method, which systematically applies the multi-level optimization strategies detailed in Section 4.

5.1.3 Performance Metrics. We employ a combination of macroscopic and microscopic performance metrics for a multi-faceted evaluation. The most direct measure of end-to-end performance is the **Total Time**, representing the wall-clock time consumed by core computational tasks. To evaluate spatial efficiency, we measure the **Memory Usage**, which is the peak memory footprint reached during execution. The solver’s overall processing capability is assessed using **Solver Throughput (MDof/s)**, calculated as the total degrees of freedom processed per second. Finally, to reflect the efficiency in utilizing hardware’s computational cores, we measure the **Computational Throughput (GFLOPS)**.

5.1.4 Benchmark Problem. All experiments solve a standard 3D linear elasticity problem, a typical application in structural mechanics and engineering simulation. The computational domain is discretized into a structured mesh of trilinear hexahedral elements, with Dirichlet boundary conditions applied to specific model surfaces. To evaluate performance under varying conditions, we vary the polynomial degree p of the basis functions from 1 to 8, allowing us to study the performance trends of the algorithms as p increases from low to high orders.

5.2 Preconditioner Performance Comparison

To ensure that subsequent evaluations of operator performance are based on a fair and efficient baseline, this section aims to validate and select an optimal preconditioning strategy. Since matrix-free methods cannot directly use standard Algebraic Multigrid (AMG) and a simple Jacobi preconditioner has poor convergence, we introduce Geometric Multigrid

(GMG) in Section 3 as a unified solution. We compare four combinations: the classic **FA + AMG**, the basic **PA + Jacobi**, and our proposed GMG applied to both full and partial assembly, **FA + GMG** and **PA + GMG**.

Table 2. Preconditioner End-to-End Performance on the 830k DoF Problem. Iteration counts and total time (in seconds) are reported. Speedup is calculated as Total Time (Baseline) / Total Time (GMG).

Order	Platform	Full Assembly (FA)						Partial Assembly (PA)					
		Iters	Total (s)	Iters	Total (s)	Speedup	Iters	Total (s)	Iters	Total (s)	Speedup		
			(AMG)	(AMG)	(GMG)	(GMG)		(Jacobi)	(Jacobi)	(GMG)	(GMG)		
1	ARM	47	2.22	6	0.61	3.64x	915	17.23	6	1.37	12.58x		
	AMD	53	3.87	6	1.02	3.79x	915	23.32	6	1.82	12.81x		
2	ARM	52	4.53	7	1.15	3.94x	1195	8.85	7	0.65	13.62x		
	AMD	52	7.08	7	1.75	4.05x	1195	12.58	7	1.04	12.10x		
4	ARM	47	17.28	9	6.25	2.76x	1548	4.77	9	0.67	7.12x		
	AMD	47	27.56	9	9.03	3.05x	1548	25.54	9	1.34	19.06x		
8	ARM	49	515.68	12	470.21	1.10x	1937	4.28	12	2.93	1.46x		
	AMD	51	751.29	12	677.56	1.11x	1937	108.86	12	5.13	21.22x		

Table 2 presents a detailed performance comparison on a medium-scale problem (0.83 million DoFs). The results clearly show that our GMG preconditioner offers outstanding convergence, reducing solver iteration counts by nearly one to three orders of magnitude compared to the respective baselines. This sharp reduction in iterations translates directly into significant total time savings. For instance, FA+GMG and PA+GMG achieved end-to-end speedups of up to 4.05x and 21.22x, respectively, proving the overwhelming performance advantage of the GMG strategy on this problem size.

Furthermore, tests on a large-scale problem of 6.5 million DoFs revealed that the performance advantage of GMG was significantly amplified at a larger scale. For example, on the AMD platform at $p = 8$, the end-to-end speedup of PA+GMG over PA+Jacobi jumped from 21.22x to 46.28x, demonstrating the superior competitiveness of our method when tackling large-scale problems. More importantly, a significant robustness gap emerged, as the traditional FA+AMG method failed to complete the test (OOM) in the high-order case of $p = 8$ due to excessive memory consumption, while our PA+GMG method succeeded. This highlights that our combined approach resolves a fundamental bottleneck of traditional methods for large-scale, high-order problems. In summary, the experimental results provide strong evidence that our proposed GMG preconditioner holds a decisive advantage. Therefore, to isolate variables and ensure a fair comparison, all subsequent experiments will uniformly adopt GMG as the preconditioner.

5.3 Macro-performance: Breaking the Bottlenecks of Large-Scale, High-Order Computations

Having established GMG as the unified preconditioner, this section evaluates the end-to-end performance of our core contribution: the optimized matrix-free operator (PAop). We compare it against two key baselines: the traditional **Full Assembly (FA)** to demonstrate that our method can break the "memory wall", and the unoptimized **Partial Assembly (PA)** to precisely quantify the performance gains from our optimization strategies.

First, at a fixed problem size of approximately 6.5 million DoFs, we compared the total solve time and peak memory usage of FA, PA, and PAop across different polynomial degrees. Thanks to our efficient GMG preconditioner, the number of solver iterations was identical for all three methods, ensuring that any differences in time directly reflect

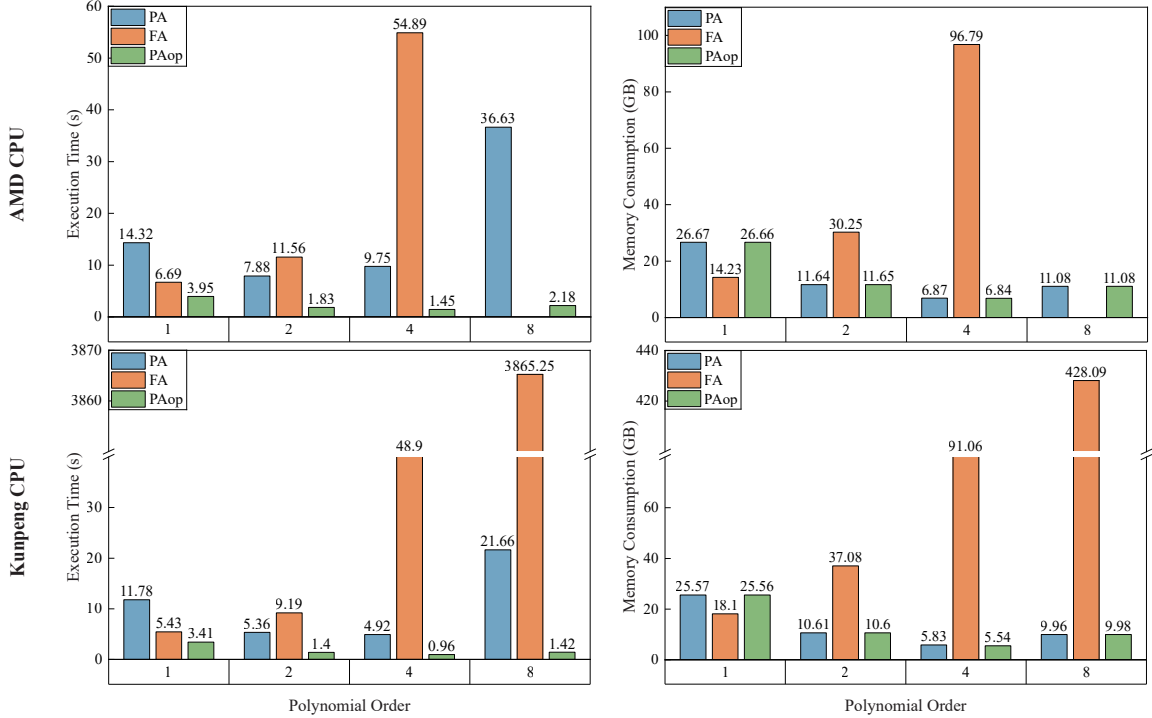


Fig. 4. Comparison of total solve time (left) and peak memory usage (right) for Full Assembly (FA), baseline Partial Assembly (PA), and our optimized operator (PAop). The experiment is conducted on a problem with approximately 6.5 million Degrees of Freedom (DoFs) while varying the polynomial degree p . Our PAop method demonstrates superior performance, achieving speedups of up to 16.8x over PA and 2722x over FA. In terms of memory, the FA method's consumption grows exponentially, whereas PA and PAop maintain a nearly constant, low memory footprint.

operator efficiency. The performance results in Figure 4 reveal several key trends. Our PAop method demonstrated an overwhelming performance advantage across all tested degrees, which became more pronounced as p increased, achieving speedups of up to 16.8x over PA and 2722x over FA. In terms of memory, the usage of the FA method exploded with increasing p , whereas the footprint of PA and PAop changed little, positioning Matrix-Free as the only viable option in high-order scenarios. Crucially, we observed that when using PAop, the fastest time-to-solution was achieved at $p = 4$, strongly challenging the conventional wisdom that "high-order methods are more expensive" and proving that with a deeply optimized operator, p -refinement can be computationally more efficient than h -refinement.

To further investigate scalability, we conducted an extreme-scale test involving approximately 51.17 million DoFs on the Kunpeng platform. The results, shown in Table 3, further reinforce our conclusions. The FA method encountered an Out-of-Memory (OOM) error for $p \geq 4$, exposing an insurmountable "capacity wall" for large-scale, high-order problems. In contrast, our PAop method not only successfully solved all test cases but also achieved a massive 15.56x speedup over its baseline PA at $p = 8$, demonstrating the excellent scalability and robustness of our optimization strategy. In summary, the PAop operator not only achieves an order-of-magnitude performance improvement but, more critically, it breaks the bottlenecks faced by the traditional FA method, greatly expanding the application boundaries of high-order finite element methods.

Table 3. Macro-performance Comparison on the 51.17M DoF Problem. All methods use the same GMG preconditioner. The total time-to-solution and peak memory usage are reported. Our proposed method, **PAop**, is highlighted in bold.

Order (p)	Algorithm	Iters	Assembly (s)	Solve (s)	Total (s)	Speedup (vs. FA)	Speedup (vs. PA)	Peak Mem. (GB)	Mem. Ratio (vs. FA)
1	PA	6	21.98	59.66	88.30	—	1.00x	196.03	—
	FA	6	45.12	9.47	59.78	1.00x	—	141.36	1.00x
	PAop	6	6.87	14.04	26.28	2.28x	3.36x	196.01	0.72x
2	PA	7	10.01	31.51	42.94	—	1.00x	78.55	—
	FA	7	93.43	24.33	118.58	1.00x	—	321.56	1.00x
	PAop	7	3.10	8.06	12.10	9.80x	3.55x	78.55	4.09x
4	PA	8	8.74	30.60	40.24	—	1.00x	39.82	—
	FA					OOM (Out of Memory)			
	PAop	8	1.79	6.19	8.38	OOM	4.80x	39.82	OOM
8	PA	11	27.06	131.56	161.00	—	1.00x	33.45	—
	FA					OOM (Out of Memory)			
	PAop	11	1.54	8.43	10.35	OOM	15.56x	33.44	OOM

5.4 Micro-performance Analysis: Uncovering the Roots of Performance Gains

While the previous section demonstrated the superiority of PAop, this section dissects the root causes of its performance gains by conducting a micro-level evaluation of the computational core, the AddMult function. The analysis here focuses on the comparison between PAop and its direct baseline PA, as they share the same algorithmic skeleton, unlike the SpMV kernel of FA.

5.4.1 Computational Throughput and Cache Behavior. Figure 5 shows the computational throughput and corresponding speedups of the PA and PAop core functions. Two distinctly different performance trajectories are clearly visible. The throughput of the baseline PA kernel drops sharply for $p > 3$, a classic cache thrashing phenomenon where the working set size exceeds the capacity of the CPU’s high-speed cache. In stark contrast, our optimized PAop kernel maintains extremely high throughput over a much wider range of orders, peaking at $p = 6$ and remaining high even at $p = 8$. This sustained efficiency is a direct result of our optimizations, which significantly reduce the working set size and improve memory locality, ultimately achieving maximum speedups of 54x and 83x on the Kunpeng and AMD processors, respectively.

5.4.2 Roofline Model-Based Bottleneck Analysis. To gain a deeper understanding of the relationship between operator performance and hardware, we plot a Roofline model[39] for the Kunpeng platform in Figure 6. The model provides two key insights. First, PAop significantly increases operational intensity, as its data points are located further to the “top-right” than the PA points, proving that our optimizations improved data locality and reduced unnecessary memory movement. Second, the model reveals the performance bottleneck. Although the performance of PAop improved substantially, it still lies on the slope determined by memory bandwidth, indicating it is primarily memory-bound, not compute-bound. This finding is critical, as it explains a seemingly counter-intuitive result from our experiments: the application performs better on the Kunpeng platform despite its lower peak floating-point performance. For a memory-bound operator like ours, the Kunpeng platform’s superior memory bandwidth becomes the decisive factor, ultimately driving the higher performance.

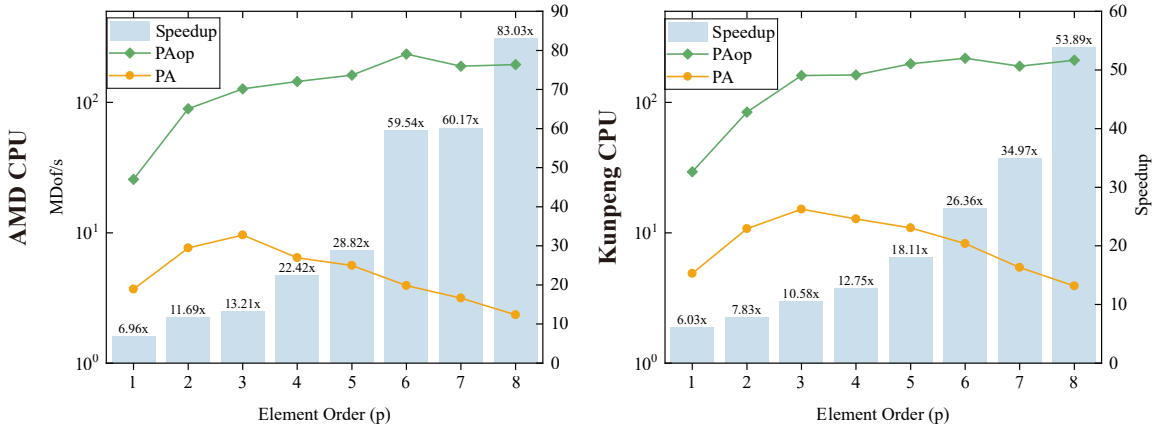


Fig. 5. Computational throughput (in MDof/s) and corresponding speedup of the baseline PA and our optimized PAop kernels on Kunpeng (left) and AMD (right) platforms. The performance of the baseline PA kernel degrades sharply for $p > 3$, a clear sign of cache thrashing as its working set exceeds the cache capacity. In contrast, our PAop kernel sustains high throughput across all polynomial degrees by improving memory locality and reducing the working set size. This results in maximum speedups of 54x on the Kunpeng platform and 83x on the AMD platform, demonstrating the effectiveness and portability of our optimization strategies.

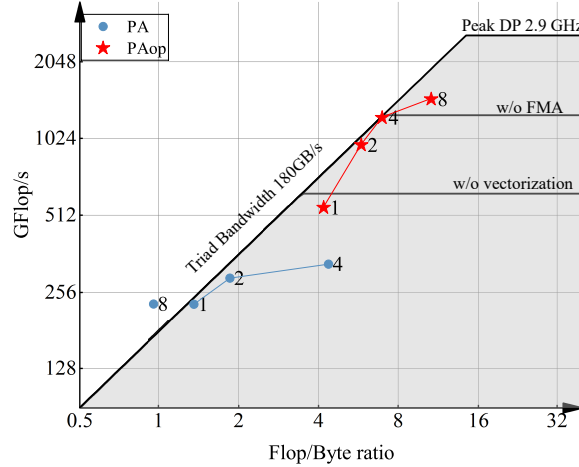


Fig. 6. Roofline model analysis of the PA and PAop kernels on the Kunpeng platform. The plot shows that our optimized PAop kernel (blue dots) significantly increases the operational intensity compared to the baseline PA (red dots), shifting the points towards the compute-bound region and confirming improved data locality. Despite the substantial performance gains, the kernel's performance points still lie on the slanted memory bandwidth ceiling, indicating that the operation remains memory-bound on this platform. This finding explains why the application performs well on hardware with high memory bandwidth.

5.5 Ablation Study

To systematically quantify the individual contribution of each optimization strategy from Section 4, we conducted an ablation study. We established a performance evolution path from the baseline to the final optimization: starting with the standard matrix-free operator (PA) as the Baseline, we then sequentially applied our key optimizations:

Sum Factorization (C1, Sec. 4.4), Voigt Notation (C2, Sec. 4.3), Kernel Fusion (C3, Sec. 4.2), and finally Loop Structure optimizations (Sec. 4.5) to arrive at the complete PAop.

All tests were conducted on the Kunpeng platform for a $p = 8$ problem with 51.17 million DoFs. Thanks to the unified GMG preconditioner, the iteration count was constant at 11 for all configurations, ensuring a fair comparison. Table 4 details the performance data, showing that our optimization strategy ultimately achieved a $54.19\times$ cumulative speedup for the kernel and a $15.65\times$ cumulative speedup for the end-to-end total time.

Table 4. Ablation study of optimization stages for the 51.17M DoF problem at $p = 8$ on the Kunpeng platform. The performance of the baseline (PA) is incrementally improved by applying successive optimizations. Marginal speedup measures the direct benefit of each single step (Time_{prev} / Time_{curr}).

Optimization Stage	End-to-End Performance		Kernel-Level Performance	
	Total Time (s)	Marginal Speedup	Kernel Time (s)	Marginal Speedup
PA (Baseline, Sec. 4.1)	161.70	—	148.47	—
+ Sum Factorization (C1, Sec. 4.4)	24.24	6.67x	11.65	12.74x
+ Voigt Notation (C2, Sec. 4.3)	19.20	1.26x	11.55	1.01x
+ Kernel Fusion (C3, Sec. 4.2)	13.00	1.48x	5.38	2.15x
+ Loop Structure (PAop, Sec. 4.5)	10.33	1.26x	2.74	1.96x
Overall Speedup (vs. Baseline)	15.65x		54.19x	

The stage-wise performance evolution detailed in Table 4 reveals a clear narrative of bottleneck migration and resolution. The foundational and most impactful optimization was the introduction of **Sum Factorization (C1)**. By fundamentally reducing the asymptotic complexity at the algorithmic level—decomposing high-dimensional tensor operations into a series of 1D operations—it yielded a remarkable $12.74\times$ marginal speedup for the kernel, single-handedly dismantling the initial computational bottleneck. The dramatic success of this first step, however, exposed a new performance limiter. The application of **Voigt Notation (C2)** was diagnostically significant: its negligible $1.01\times$ kernel speedup revealed that with the computational bottleneck gone, performance had become entirely dominated by memory bandwidth, limited by reading and writing intermediate data.

This insight provided a clear mandate for the next optimization, **Kernel Fusion (C3)**, which was designed specifically to break this "memory wall." By fusing multiple computational kernels, intermediate results (such as element gradients) that previously required round-trips to main memory could now reside in the CPU's high-speed cache. This dramatic improvement in data locality directly translated into a $2.15\times$ kernel speedup, effectively mitigating the memory bandwidth bottleneck. With the macroscopic algorithmic and memory access patterns optimized, the final stage of **Loop Optimization (PAop)** involved microarchitectural fine-tuning. This step, which included reducing intermediate arrays and improving SIMD efficiency, squeezed out the remaining hardware potential, contributing a final $1.96\times$ marginal speedup.

This ablation study clearly validates our multi-stage optimization strategy. The discrepancy between the massive $54.19\times$ kernel speedup and the $15.65\times$ total time speedup also perfectly illustrates Amdahl's Law: as the computational core is extremely optimized, its share of the total runtime shrinks, and the program's performance bottleneck gradually shifts to other parts, pointing to new directions for future optimization work.

6 Conclusion

High-order finite element methods theoretically offer an efficient path to high-precision scientific computing, yet in practice, they have long been constrained by the "memory wall" bottleneck imposed by traditional Full Assembly (FA) strategies. Matrix-free (PA) methods, combined with tensor-product elements that offer dual advantages in geometry and algorithms, provide a theoretical solution by trading memory access for computation. However, we found that the general-purpose PA implementations in mainstream finite element libraries fail to fully exploit their optimization potential. This leads to practical performance on modern multi-core CPUs that falls far short of expectations, with the performance "sweet spot" anomalously remaining in the low-order region. This constitutes the core disconnect between the theoretical advantages of high-order methods and their engineering practice when applied to complex problems such as elasticity.

This paper has systematically addressed this challenge. We first constructed a solver framework that deeply integrates the matrix-free operator with an efficient Geometric Multigrid (GMG) preconditioner, laying a solid foundation for high-performance solves. Within this framework, we replaced the original $O(p^6)$ general-purpose operator in MFEM with an $O(p^4)$ algorithm based on tensor-product factorization. On top of this, we implemented a multi-level, systematic optimization strategy—including the use of Voigt symmetry, kernel fusion, and microarchitectural loop optimizations—culminating in our optimized operator, PAop.

Exhaustive experimental evaluations provide compelling evidence for the success of our work. At the macroscopic level, PAop achieves end-to-end speedups of up to 55 \times (at $p = 4$) over the traditional FA method and up to 17 \times (at $p = 8$) over the standard PA method. It completely breaks the memory bottleneck faced by FA when solving large-scale, high-order problems, greatly expanding the solvable scale. More importantly, our work successfully shifts the performance "sweet spot" of high-order operators on CPUs from the $p \approx 2$ observed in prior work to the region of $p \geq 6$ and beyond. This shift is of significant importance, as it demonstrates in practice that, when equipped with a deeply optimized operator, a p -refinement strategy that relies on increasing polynomial degree can be computationally more efficient than an h -refinement strategy that relies on mesh densification.

Our micro-performance analysis and ablation study further reveal the underlying mechanisms of this success. We evaluated the throughput of the core operator and quantified the independent contribution of each optimization technique, proving the decisive role of tensor-product factorization at the algorithmic level and the critical value of kernel fusion in breaking the internal bandwidth bottleneck and enhancing data locality. The Roofline model analysis clarified from an architectural perspective that our optimizations significantly increase the operator's operational intensity, shifting its performance bottleneck from pure memory latency to a more complex balance between computation and memory access.

In conclusion, through synergistic optimization across the algorithmic, software, and architectural levels, this paper bridges the gap between the theory and practice of high-order matrix-free methods. It provides a fully validated and reproducible solution for efficiently solving large-scale, high-order linear elasticity problems on mainstream CPU architectures.

Although this work has achieved significant performance improvements, our analysis also points to several promising directions for future research:

- (1) **Mixed-Precision Computing:** This work was based on double-precision (FP64) arithmetic. We observed that although the computational intensity of the optimized operator increased significantly, memory bandwidth pressure remains a limiting performance factor. Exploring a mixed-precision strategy, where parts of the

computation (such as the preconditioner application) are moved to half-precision (FP16) or single-precision (FP32), holds the promise of achieving up to a 2x performance boost by further squeezing hardware performance, without significantly affecting convergence.

- (2) **Extension to More Complex Physics Models:** This work focused on the linear elasticity problem. Extending these optimization principles and methodologies for tensor-product elements to other, more complex physics models—such as non-linear solid mechanics, fluid dynamics (Navier-Stokes equations), or electromagnetics (Maxwell’s equations)—would be a highly valuable next step.
- (3) **Further Optimization of System-Level Bottlenecks:** As Amdahl’s Law dictates, with our extreme optimization of the computational kernel, the system’s overall bottleneck has gradually shifted to other components, such as the coarse-grid solve in GMG, parallel communication, and other auxiliary computations. Targeting these new bottlenecks is key to achieving continuous improvement in the solver’s overall performance.

References

- [1] Ahmad Abdelfattah, Valeria Barra, Natalie Beams, Ryan Bleile, Jed Brown, Jean-Sylvain Camier, Robert Carson, Noel Chalmers, Veselin Dobrev, Yohann Dudouit, et al. 2021. GPU algorithms for efficient exascale discretizations. *Parallel Comput.* 108 (2021), 102841.
- [2] Robert Anderson, Julian Andrej, Andrew Barker, Jamie Bramwell, Jean-Sylvain Camier, Jakub Cerveny, Veselin Dobrev, Yohann Dudouit, Aaron Fisher, Tzanio Kolev, et al. 2021. MFEM: A modular finite element methods library. *Computers & Mathematics with Applications* 81 (2021), 42–74.
- [3] Julian Andrej, Nabil Atallah, Jan-Phillip Bäcker, Jean-Sylvain Camier, Dylan Copeland, Veselin Dobrev, Yohann Dudouit, Tobias Duswald, Brendan Keith, Dohyun Kim, et al. 2024. High-performance finite elements with MFEM. *The International Journal of High Performance Computing Applications* 38, 5 (2024), 447–467.
- [4] Daniel Arndt, Wolfgang Bangerth, Maximilian Bergbauer, Marco Feder, Marc Fehling, Johannes Heinz, Timo Heister, Luca Heltai, Martin Kronbichler, Matthias Maier, et al. 2023. The deal. II library, version 9.5. *Journal of Numerical Mathematics* 31, 3 (2023), 231–246.
- [5] Satish Balay, Shrirang Abhyankar, Mark Adams, Jed Brown, Peter Brune, Kris Buschelman, Lisandro Dalcin, Alp Dener, Victor Eijkhout, William Gropp, et al. 2019. PETSc users manual. (2019).
- [6] SS Bhavikatti. 2005. *Finite element analysis*. New Age International.
- [7] Jed Brown, Ahmad Abdelfattah, Valeria Barra, Natalie Beams, Jean-Sylvain Camier, Veselin Dobrev, Yohann Dudouit, Leila Ghaffari, Tzanio Kolev, David Medina, et al. 2021. libCEED: Fast algebra for high-order element-based discretizations. *Journal of Open Source Software* 6, 63 (2021), 2945.
- [8] Jed Brown, Valeria Barra, Natalie Beams, Leila Ghaffari, Matthew Knepley, William Moses, Rezgar Shakeri, Karen Stengel, Jeremy L Thompson, and Junchao Zhang. 2022. Performance Portable Solid Mechanics via Matrix-Free p -Multigrid. *arXiv preprint arXiv:2204.01722* (2022).
- [9] Zijian Cao, Qiao Sun, Tiangong Zhang, and Huiyuan Li. 2025. Towards a Higher Roofline for Matrix-Vector Multiplication in Matrix-Free HOSFEM. *arXiv preprint arXiv:2504.07042* (2025).
- [10] GF Carey, E Barragy, R McLay, and M Sharma. 1988. Element-by-element vector and parallel computations. *Communications in Applied Numerical Methods* 4, 3 (1988), 299–307.
- [11] Graham F Carey and Bo-Nan Jiang. 1986. Element-by-element linear and nonlinear solution schemes. *Communications in Applied Numerical Methods* 2, 2 (1986), 145–153.
- [12] P Pal Chaudhuri. 2008. *Computer organization and design*. PHI Learning Pvt. Ltd.
- [13] Thomas C Cleverger, Timo Heister, Guido Kanschat, and Martin Kronbichler. 2020. A flexible, parallel, adaptive geometric multigrid method for FEM. *ACM Transactions on Mathematical Software (TOMS)* 47, 1 (2020), 1–27.
- [14] Arnaldo Carvalho De Melo. 2010. The new linux’perf’tools. In *Slides from Linux Kongress*, Vol. 18.
- [15] Michel O Deville, Paul F Fischer, and Ernest H Mund. 2002. *High-order methods for incompressible fluid flow*. Vol. 9. Cambridge university press.
- [16] Robert D Falgout and Ulrike Meier Yang. 2002. hypre: A library of high performance preconditioners. In *International Conference on computational science*. Springer, 632–641.
- [17] Serban Georgescu, Peter Chow, and Hiroshi Okuda. 2013. GPU acceleration for FEM-based structural analysis. *Archives of Computational Methods in Engineering* 20, 2 (2013), 111–121.
- [18] Nitin S Gokhale. 2008. *Practical finite element analysis*. Finite to infinite.
- [19] Johnnie Gray and Garnet Kin-Lic Chan. 2024. Hyperoptimized approximate contraction of tensor networks with arbitrary geometry. *Physical Review X* 14, 1 (2024), 011009.
- [20] William D Gropp, Dinesh K Kaushik, David E Keyes, and Barry F Smith. 1999. Toward realistic performance bounds for implicit CFD codes. In *Proceedings of parallel CFD*, Vol. 99. 233–240.
- [21] Thomas JR Hughes, John A Cottrell, and Yuri Bazilevs. 2005. Isogeometric analysis: CAD, finite elements, NURBS, exact geometry and mesh refinement. *Computer methods in applied mechanics and engineering* 194, 39-41 (2005), 4135–4195.

- [22] George Karniadakis and Spencer Sherwin. 2013. *Spectral/hp element methods for computational fluid dynamics*. Oxford University Press, USA.
- [23] Martin Karp, Artur Podobas, Tobias Kenter, Niclas Jansson, Christian Plessl, Philipp Schlatter, and Stefano Markidis. 2022. A high-fidelity flow solver for unstructured meshes on field-programmable gate arrays: Design, evaluation, and future challenges. In *International Conference on High Performance Computing in Asia-Pacific Region*. 125–136.
- [24] Martin Kronbichler and Katharina Kormann. 2012. A generic interface for parallel cell-based finite element operator application. *Computers & Fluids* 63 (2012), 135–147.
- [25] Martin Kronbichler and Katharina Kormann. 2019. Fast matrix-free evaluation of discontinuous Galerkin finite element operators. *ACM Transactions on Mathematical Software (TOMS)* 45, 3 (2019), 1–40.
- [26] Martin Kronbichler and Karl Ljungkvist. 2019. Multigrid for matrix-free high-order finite element computations on graphics processors. *ACM Transactions on Parallel Computing (TOPC)* 6, 1 (2019), 1–32.
- [27] Xianyang Liu, Qunwei Wang, Yongwei Wang, and Qinxi Dong. 2023. Review of calibration strategies for discrete element model in quasi-static elastic deformation. *Scientific Reports* 13, 1 (2023), 13264.
- [28] Karl Ljungkvist. 2014. Matrix-free finite-element operator application on graphics processing units. In *European Conference on Parallel Processing*. Springer, 450–461.
- [29] Karl Ljungkvist. 2017. *Finite element computations on multicore and graphics processors*. Ph.D. Dissertation. Acta Universitatis Upsaliensis.
- [30] Karl Ljungkvist. 2019. Matrix-free finite-element computations on graphics processors with adaptively refined unstructured meshes. In *Proceedings of the 25th High Performance Computing Symposium*. 1–12.
- [31] Arash Mehrabian, Henry Tufo, Stein Sture, and Richard Regueiro. 2021. Matrix-Free Higher-Order Finite Element Method for Parallel Simulation of Compressible and Nearly-Incompressible Linear Elasticity on Unstructured Meshes. *Computer Modeling in Engineering & Sciences (CMES)* 129, 3 (2021).
- [32] Steven A Orszag. 1979. Spectral methods for problems in complex geometries. In *Numerical methods for partial differential equations*. Elsevier, 273–305.
- [33] Steven J Owen. 1998. A survey of unstructured mesh generation technology. *IMR* 239, 267 (1998), 15.
- [34] Les Piegl and Wayne Tiller. 2012. *The NURBS book*. Springer Science & Business Media.
- [35] pigirons. 2022. *cpufp: A CPU tool for benchmarking the peak of floating points*. <https://github.com/pigirons/cpufp> Accessed: 2025-09-29.
- [36] Richard Schussnig, Niklas Fehn, Peter Munch, and Martin Kronbichler. 2025. Matrix-free higher-order finite element methods for hyperelasticity. *Computer Methods in Applied Mechanics and Engineering* 435 (2025), 117600.
- [37] Jan Treibig, Georg Hager, and Gerhard Wellein. 2010. Likwid: A lightweight performance-oriented tool suite for x86 multicore environments. In *2010 39th international conference on parallel processing workshops*. IEEE, 207–216.
- [38] Yi-Yao Wang, Qiwei Zhan, Haoqiang Feng, Yin-Da Wang, Bozhao Sun, and Wen-Yan Yin. 2024. A Novel Matrix-Free Finite Element Method for Time-Harmonic Maxwell's Equations. *IEEE Transactions on Antennas and Propagation* 72, 3 (2024), 2609–2619.
- [39] Samuel Williams, Andrew Waterman, and David Patterson. 2009. Roofline: an insightful visual performance model for multicore architectures. *Commun. ACM* 52, 4 (2009), 65–76.
- [40] Qimen Xu, Abhiraj Sharma, Benjamin Comer, Hua Huang, Edmond Chow, Andrew J Medford, John E Pask, and Phanish Suryanarayana. 2021. SPARC: Simulation package for ab-initio real-space calculations. *SoftwareX* 15 (2021), 100709.